Hydrogen Bond and π-π Stacking Interaction: Stabilization Mechanism of Two Metal *Cyclo*-N$_5^-$-Containing Energetic Materials

Xiang Li, Yao Long, Chong Zhang, Chengguo Sun, Bingcheng Hu, Pengfei Lu,* and Jun Chen*

ACCESS | Metrics & More | Article Recommendations

ABSTRACT: In recent years, *cyclo*-N$_5^-$ has attracted extensive attention because all-nitrogen high-energy-density materials (HEDMs) have been expected to reach a TNT equivalent of over 3.0. However, for *cyclo*-N$_5^-$-containing HEDMs, the stabilization mechanism has remained enigmatic. In this study, two typical *cyclo*-N$_5^-$-containing metal hydrates, $[Na(H_2O)(N_5)]\cdot 2H_2O$ (Na-*cyclo*-N$_5^-$) and $[Mg(H_2O)_6(N_5)_2]\cdot 4H_2O$ (Mg-*cyclo*-N$_5^-$), are selected to gain insights into the factors affecting their stability by the first-principles method. Both binding/lattice energy calculations and density of states analysis show that Mg-*cyclo*-N$_5^-$ is more stable than Na-*cyclo*-N$_5^-$. Hydrogen bonding is the main stabilization mechanism for stabilizing crystals and *cyclo*-N$_5^-$. Two types of hydrogen bonds, O−H···O and O−H···N, are clarified, which construct a 3D hydrogen bond network in Mg-*cyclo*-N$_5^-$ and an intralayer 2D hydrogen bond network in Na-*cyclo*-N$_5^-$. Moreover, nonuniform stress causes distortion of *cyclo*-N$_5^-$. Comparing the two samples, the distortion degree of *cyclo*-N$_5^-$ is higher in Na-*cyclo*-N$_5^-$, which indicates that *cyclo*-N$_5^-$ decomposition is easier. These findings will enhance the future prospects for the design and synthesis of *cyclo*-N$_5^-$-containing HEDMs.
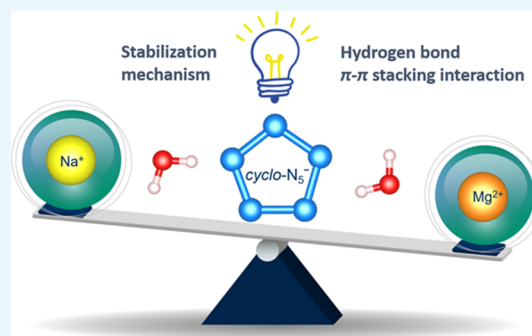
1. INTRODUCTION

Nitrogen-rich high-energy-density materials (HEDMs) are gaining popularity due to their excellent energy storage capacity and environmentally friendly decomposition products.[1−5] Because of possessing a large number of N−N, N=N, and N≡N bonds, nitrogen-rich materials contain higher energy (38.2, 99.9, and 224.9 kcal mol^{-1} for N−N, N=N, and N≡N, respectively) than traditional CHON explosives (C−C, C−N, C=C, and C≡C bonds).[6] In the past few decades, a few nitrogen-rich HEDMs, such as azide salts: N$_3^-$,[7,8] N$_3^+$,[7,8] N$_4^+$,[9] and N$_5^{+}$[10−12] salts; metastable molecules: tetraazatetrahedrane (N$_4$),[13] hexaazabenzene (N$_6$),[13,14] and octaazacubane (N$_8$);[13] single-bonded cubic form of nitrogen: cg−N,[15] and so forth, have been researched and synthesized. Several theoretical studies had also contributed to the synthesis of more diversified stable nitrogen-rich HEDMs.[16−18]

Among the nitrogen-rich HEDMs, the five-membered *cyclo*-N$_5^-$ ring has a unique structure and a greater ability to store energy compared to the azide ions. However, the synthesis of *cyclo*-pentazole (*cyclo*-N$_5^-$) HEDMs, which are stable in common conditions, remains a challenge. In fact, attempts were made to synthesize *cyclo*-N$_5^-$ at a very early stage.[19−21] However, *cyclo*-N$_5^-$ obtained from the experimentally synthesized scheme is short-lived, unstable under normal conditions, and extremely susceptible to decomposition into dinitrogen (N$_2$) and N$_3^-$ (the decomposition of *cyclo*-N$_5^-$ into N$_2$ and N$_3^-$ is exothermic by 14.3 kcal mol^{-1}, and the activation energy for

this decomposition is 27.2 kcal mol^{-1}.[4]). Therefore, a stabilization mechanism of *cyclo*-N$_5^-$ has always been a key issue in such exploration in *cyclo*-N$_5^-$ HEDMs. Until recently, an experimentally workable method was used for the synthesis of stable *cyclo*-N$_5^-$-containing HEDMs. In 2017, the first stable nonmetallic *cyclo*-N$_5^-$ salt in common conditions, (N$_5$)$_6$(H$_3$O)$_3$(NH$_4$)$_4$Cl (PHAC), was synthesized by Zhang et al.[22] It is a brilliant achievement after more than 50 years of unremitting effort and opens the door to the extensive development of pentazolate chemistry.[23] However, 1.340 g cm^{-3} density of this material and dilution with nonenergetic components did not meet the demands of HEDMs. To produce pentazolate (*cyclo*-N$_5^-$) compounds with relatively high performance while maintaining thermal stability, metal ions and/or high-nitrogen-containing cations were investigated as *cyclo*-N$_5^-$ traps.[24] Then, [Co(N$_5$)$_2$(H$_2$O)$_4$]·4H$_2$O, an air-stable orange metal complex, was synthesized by reacting (N$_5$)$_6$(H$_3$O)$_3$(NH$_4$)$_4$Cl and [Co(NO$_3$)$_2$]·6H$_2$O at room temperature.[24] Immediately after that, a series of stable high-

energy metal pentazolate hydrates, $[Na(H_2O)(N_5)]\cdot 2H_2O$ (Na-$cyclo$-N_5^-), $[M(H_2O)_4(N_5)_2]\cdot 4H_2O$ (M = Mn, Fe and Co), and $[Mg(H_2O)_6(N_5)_2]\cdot 4H_2O$ (Mg-$cyclo$-N_5^-), was synthesized by Xu et al.[25] Furthermore, they also synthesized some other nitrogen-rich HEDMs within $cyclo$-N_5^-, such as $[Zn\text{-}(N_5)_2(H_2O)_4]\cdot 4H_2O$[26] and three anhydrous and metal-free energetic salts.[27]

Among such $cyclo$-N_5^- materials, $cyclo$-N_5^- metal hydrates are particularly interesting. In the classical theoretical calculation method (Kamlet−Jacobs theory) of detonation properties, such as detonation pressure, detonation velocity, and detonation heat, density is a basic parameter. Synthesizing energetic materials (EMs) with higher density is an important way to improve the detonation performance. Therefore, the addition of metal elements in $cyclo$-N_5^- metal hydrates will not only effectively increase the density but also help obtain the $cyclo$-N_5^- EMs with relatively high performance. How to sustain or even improve the stability of metal hydrate is very necessary for its subsequent application. In the synthesized $cyclo$-N_5^- metal hydrate mentioned above, there are two ways to capture $cyclo$-N_5^-: one is that the metal cations are coordinated with $cyclo$-N_5^-; the other is that the metal cations are not directly connected with $cyclo$-N_5^- but form hydrogen bonds (HBs) with $cyclo$-N_5^- through surrounding coordination H_2O molecules. Mg-$cyclo$-N_5^- is only one of these metal hydrates in which $cyclo$-N_5^- are nonbonding with the metal atoms.[25] Metal atoms in other metal hydrates are all bonded with $cyclo$-N_5^-, such as Na-$cyclo$-N_5^-, $[M(H_2O)_4(N_5)_2]\cdot 4H_2O$ (M = Mn, Fe, and Co),[25] and $[Zn(N_5)_2(H_2O)_4]\cdot 4H_2O$.[26] However, the stabilization mechanism of such novel $cyclo$-N_5^- metal hydrates has not been explored in depth so far.

Among the metal hydrates, $[Na(H_2O)(N_5)]\cdot 2H_2O$ (Na-$cyclo$-N_5^-) and $[Mg(H_2O)_6(N_5)_2]\cdot 4H_2O$ (Mg-$cyclo$-N_5^-) are not only the representatives of two types of stabilizing $cyclo$-N_5^- (whether the $cyclo$-N_5^- form coordination bonds with metal atoms), but also two typical $cyclo$-N_5^- precursors. As reported, Na-$cyclo$-N_5^- was the first metal hydrate successfully synthesized, while the other four $cyclo$-N_5^- energetic metal hydrates were synthesized by substituting Na^+ therein.[25] The 3D framework metal hydrate, $[Na_8(N_5)_8(H_2O)_3]_n$, was also synthesized by Na-$cyclo$-N_5^-.[28] Therefore, Na-$cyclo$-N_5^- is considered to be a vital precursor for the synthesis of metal hydrates. AgN_5 was synthesized reactively by adding $AgNO_3$ to Mg-$cyclo$-N_5^-.[29] In addition, a series of nonmetallic $cyclo$-N_5^--containing energetic salts, such as NH_4N_5, NH_3OHN_5, and $N_2H_5N_5$, had also been synthesized from Mg-$cyclo$-N_5^-.[30] Obviously, Mg-$cyclo$-N_5^- can also act as a precursor to form $cyclo$-N_5^--containing compounds, especially for nonmetallic $cyclo$-N_5^- energetic salts. Therefore, the two representative samples, Na-$cyclo$-N_5^- and Mg-$cyclo$-N_5^-, are selected to explore the factors affecting their stability.

A HB network is considered the main stabilization factor for nonmetallic $cyclo$-N_5^- energetic salts.[31] However, for such $cyclo$-N_5^- metal hydrates, the stabilization mechanism is unclear, and the related investigation is lacking. In the present work, therefore, we employed the first-principles method to investigate the crystalline packing and stability of Na-$cyclo$-N_5^- and Mg-$cyclo$-N_5^-.[32−34] Both formation/binding energy calculations and density of states (DOS) analysis show that Mg-$cyclo$-N_5^- is more stable than Na-$cyclo$-N_5^-. In Na-$cyclo$-N_5^-, $cyclo$-N_5^- is stabilized by two Na ↔ N ion bonds and three O−H···N HBs. In Mg-$cyclo$-N_5^-, $cyclo$-N_5^- is completely stabilized by weak interaction: five O−H···N HBs and π-π stacking interactions. Instead of

enhancing the stability of Na-$cyclo$-N_5^-, the Na ↔ N ion bonds make $cyclo$-N_5^- nonuniformly stressed, resulting in its easy decomposition. The five HBs in Mg-$cyclo$-N_5^- make $cyclo$-N_5^- uniformly stressed and less distorted, which improves its stability. In addition, the 2D HB network in Na-$cyclo$-N_5^- and the 3D HB network in Mg-$cyclo$-N_5^- are of great significance to enhance the stability. The 3D HB network is superior to the 2D HB network. In summary, we gain insights into the stabilization mechanism from $cyclo$-N_5^--containing HEDMs that have been successfully prepared and frequently used, and our findings will provide a good reference for the future design and synthesis of such novel, stable, $cyclo$-N_5^--containing HEDMs.

2. COMPUTATIONAL METHODS

All the first-principle calculations and lattice dynamics calculations were performed with a self-developed package, the High Accuracy atomistic Simulation package for Energetic Materials (HASEM).[32,33] The reliability of the HASEM program to describe the structures, energetics, dynamics, mechanical properties, detonation performance, and sensitivity of EM crystals has been extensively verified by comparison of the results with experiments and with CCSD(T) results.[33−35,39] To better verify its reliability in describing the noncovalent interactions and structure of the molecules in this paper, we computed CCSD(T) results for comparison. As shown in Table 1, we selected cluster models of the two samples studied in this

Table 1. Comparison between CCSD(T) and HASEM

	cluster structure	method	binding energy (kcal mol^{-1})	error (%)
$Na(H_2O)(N_5)$		CCSD(T)	−94.82	−1.25
		HASEM	−93.63	
$Mg(H_2O)_6(N_5)_2$		CCSD(T)	−95.42	−1.04
		HASEM	−94.43	

paper and calculated their energy with CCSD(T) and HASEM. The level of CCSD(T) in terms of the basis set is def2-QZVP. The calculation level of HASEM is Perdew−Burke−Ernzerhof (PBE), and D3-BJ intermolecular dispersion correction was adopted. Binding energy was calculated according to formula 1 in Section 3.1. It can be seen that the errors between the results of HASEM and CCSD(T) were very small, approximately −1%, which was sufficient to illustrate the accuracy of the calculated HASEM results.

The two Na-$cyclo$-N_5^- and Mg-$cyclo$-N_5^- bulk materials were simulated using a $1 \times 1 \times 1$ unit cell. Figure 1 shows the bulk models of Na-$cyclo$-N_5^- and Mg-$cyclo$-N_5^-. The Na-$cyclo$-N_5^- models along a and c directions are shown in Figure 1a,b, respectively. In Na-$cyclo$-N_5^-, there are totally 60 atoms: 4 Na^+, 4 N_5^-, and 12 H_2O. Five N atoms in $cyclo$-N_5^- are perfectly coplanar along the b axis. $Cyclo$-N_5^- rings are directly connected to Na and form N ↔ Na ion bonds. Na is a six-coordination atom in Na-$cyclo$-N_5^-, which is bonded with two $cyclo$-N_5^- and four H_2O molecules. Figure 1c,d show the Mg-$cyclo$-N_5^- models along the a and c axes, respectively. In Mg-$cyclo$-N_5^-, there are 41 atoms: 1 Mg^{2+}, 2 N_5^-, and 10 H_2O. Five N atoms in $cyclo$-N_5^- are also coplanar. $cyclo$-N_5^- are not directly bonded with Mg. Similar to Na-$cyclo$-N_5^-, in Mg-$cyclo$-N_5^-, Mg is also a six-coordination atom, and each Mg is bonded with six H_2O molecules.

The specific settings for the structure optimization of these two crystals are set as follows. Monkhorst-Pack k-point nets of 3 $\times$ 2 $\times$ 3 and 3 $\times$ 3 $\times$ 3 were chosen to sample the reciprocal
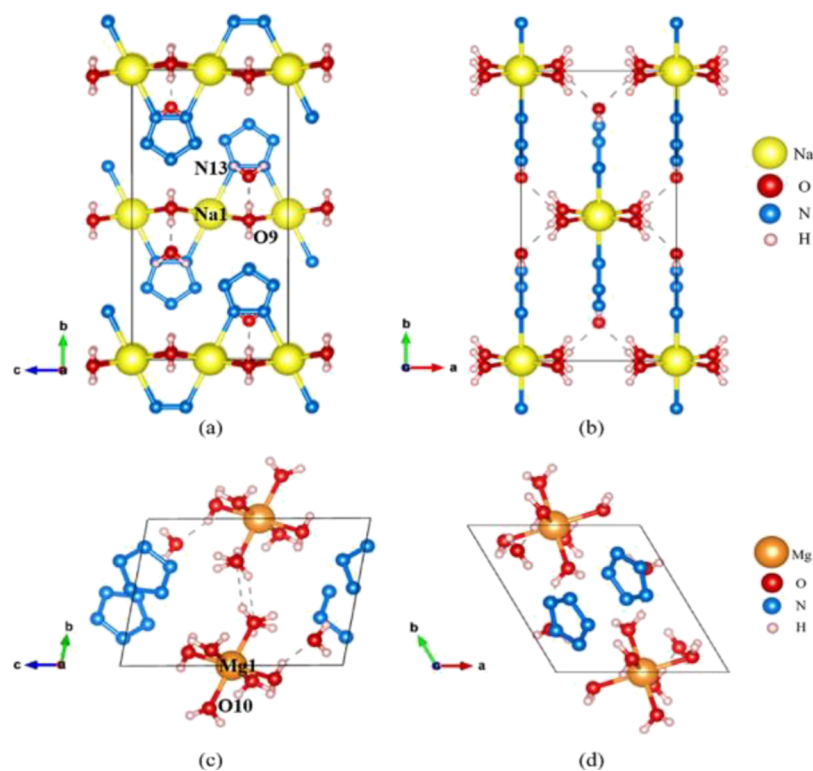
Figure 1. Structure models of Na-*cyclo*-N$_5^-$ and Mg-*cyclo*-N$_5^-$. (a, b) Views of the Na-*cyclo*-N$_5^-$ model, along *a* and *c* axes, respectively. (c, d) Views of the Mg-*cyclo*-N$_5^-$ model, along a and c axes, respectively. Na is shown in yellow, Mg is shown in orange, O is shown in red, N is shown in blue, and H is shown in white.

Table 2. Crystal Data for Na-*cyclo*-N$_5^-$ and Mg-*cyclo*-N$_5^-$

		a (Å)	*b* (Å)	*c* (Å)	*α* (°)	*β* (°)	*γ* (°)	*V* (Å^3)	*d* (g cm^{-3})
Na-*cyclo*-N$_5^-$	calc.	6.85	13.84	7.02	90	90	90	665.52	1.473
	expt.[25]	6.91	13.87	6.93	90	90	90	664.00	1.471
	error (%)	−0.87	−0.22	1.29	0	0	0	0.23	0.14
Mg-*cyclo*-N$_5^-$	calc.	7.17	7.23	8.90	91.27	103.97	118.55	388.18	1.48
	expt.[25]	7.18	7.20	9.26	90.77	107.12	117.68	398.28	1.44
	error (%)	−0.14	0.42	−3.89	0.55	−2.94	0.74	−2.54	2.78

space. Electronic state occupancy obeys the Methfessel and Paxton distribution.[36] General gradient approximation with a PBE functional was adopted to describe the electron correlation.[37−39] Core electrons were replaced by nonlocal norm-conserving pseudopotentials,[40,41] and the valence electrons were described by linear combinations of 18 numerical pseudoatomic orbitals. The large number of valence electron orbitals can ensure that the valence electrons have enough transition space, so that higher energy calculation accuracy can be achieved. The cutoff energy was chosen to be 6802.9 eV to ensure the convergence accuracy of the electrons. D3-BJ intermolecular dispersion correction was adopted. The initial lattice parameters and atomic coordinates obtained from single-crystal X-ray diffraction analysis are used as inputs for geometric optimization based on the conjugate gradient method. The optimization will be accomplished by following the condition that charge density matrix convergence criterion limit is at 5×10^{-6} and energy convergence criterion is at 10^{-4} eV. Moreover, the simulated structure was finally optimized when the residual forces were less than 0.04 eV/Å and the stress components were less than 0.01 GPa. The simulated structures of Na-*cyclo*-N$_5^-$ and Mg-*cyclo*-N$_5^-$ (Figure 1 and Table 2) show satisfactory agreement with the characterized structure by X-ray diffraction,

with the discrepancy of the volume at 0.2 and −2.5%, the discrepancy of lattice vectors at ∼1 and ∼3%, and the discrepancy of density at 0.1 and 2.8%. It can be seen that the error between the result calculated by HASEM and the experimental data was very small, which was sufficient to illustrate the accuracy of the calculated HASEM results.

3. RESULTS AND DISCUSSION

3.1. Binding/Lattice Energy and Structure Characteristic of Crystals. The theoretically calculated binding energy and lattice energy are adopted to analyze the stability of these two crystals from the perspective of energetics. Binding energy is defined as the difference between the total energy of constituent atoms in the free state and the total energy of the crystal, as shown in formula 1. The larger the absolute value of the binding energy, the more stable the compound is.

$$\text{BE} = \frac{1}{a + b + c \cdots}(E_{\text{crystal}}^{\text{total}} - aE_{\text{atom}_1}^{\text{total}} - bE_{\text{atom}_2}^{\text{total}} - cE_{\text{atom}_3}^{\text{total}} \cdots) \tag{1}$$

a, *b*, and *c* represent the number of atom$_1$, atom$_2$, and atom$_3$ in the crystal, respectively. As shown in Table 3, the absolute value

Table 3. Bond and Angle of *Cyclo*-N$_5^-$; Free Energy, Binding Energy (BE), and Lattice Energy (LE) for Na-*cyclo*-N$_5^-$ and Mg-*cyclo*-N$_5^-$

	d_{N-N} (Å)	a_{N-N-N} (c)	free energy (kcal·mol^{-1})	BE (kcal·mol^{-1})	LE (kcal·mol^{-1})
Na-*cyclo*-N$_5^-$	1.31~1.33	107.89~108.25	−254,738.6	−125.2	186.7
Mg-*cyclo*-N$_5^-$	1.31~1.32	107.88~108.20	−172,266.4	−138.0	244.2

of the binding energy of Mg-*cyclo*-N$_5^-$ is 12.8 kcal·mol^{-1} greater than that of Na-*cyclo*-N$_5^-$ (−138.0 kcal·mol^{-1} for Mg-*cyclo*-N$_5^-$ and −125.2 kcal·mol^{-1} for Na-*cyclo*-N$_5^-$). Lattice energy is defined as the difference between the total energy of constituent ions in the free state and the total energy of the crystal in the free state, as shown in formula 2. The larger the value of the lattice energy, the more stable the compound is.

$$LE = E_{crystal}^{total} - \sum_{i=1}^{n} E_i^{total} \tag{2}$$

The calculated lattice energy of NaCl was 182.4 kcal·mol^{-1}, which is consistent with the reported 187.9 kcal·mol^{-1}, with an error of −2.92%.[42] The small discrepancy confirmed the reliability of the current calculation. As shown in Table 3, Na-*cyclo*-N$_5^-$ had a comparable lattice energy (186.7 kcal·mol^{-1}) with a NaCl crystal (187.9 kcal·mol^{-1}). The calculated lattice energy of Mg-*cyclo*-N$_5^-$ is 57.5 kcal·mol^{-1} greater than that of Na-*cyclo*-N$_5^-$ (244.2 kcal·mol^{-1} for Mg-*cyclo*-N$_5^-$ and 186.7 kcal·mol^{-1} for Na-*cyclo*-N$_5^-$). Both of these two energy values clearly indicate that Mg-*cyclo*-N$_5^-$ is more stable than Na-*cyclo*-N$_5^-$. However, in Na-*cyclo*-N$_5^-$, *cyclo*-N$_5^-$ is stabilized by the N ↔ Na ion bond, while in Mg-*cyclo*-N$_5^-$, *cyclo*-N$_5^-$ is not bonded with other ions, but stabled by HBs. Logically, the former (Na-*cyclo*-N$_5^-$) should be more stable. Therefore, this is a very interesting finding, and the factors affecting their stability need to be further analyzed.

For *cyclo*-N$_5^-$-containing EMs, the structure and stability of *cyclo*-N$_5^-$ have always been the focus of attention. As demonstrated in Figure 2a, the undistorted *cyclo*-N$_5^-$ is a perfect

Figure 2. Structure of *cyclo*-N$_5^-$. (a) Minimum energy structure of *cyclo*-N$_5^-$.[6] (b, c) *cyclo*-N$_5^-$ of Na-*cyclo*-N$_5^-$ and Mg-*cyclo*-N$_5^-$, respectively. Longest N−N bonds are shown in red. Maximum N−N−N angles are shown in blue.

regular pentagon, and the most stable structure possesses five N−N bonds of 1.33 Å and five N−N−N angles of 108°.[6] In Table 3, we list the N−N bond length (BL) and N−N−N angles of *cyclo*-N$_5^-$ in two samples. The N−N bonds are 1.31~1.33 Å in Na-*cyclo*-N$_5^-$ and 1.31~1.32 Å in Mg-*cyclo*-N$_5^-$. Compared with the undistorted *cyclo*-N$_5^-$, when *cyclo*-N$_5^-$ is located in the crystal, the BLs are slightly shorter and unequal. The N−N−N angles are 107.89~108.25° in Na-*cyclo*-N$_5^-$ and 107.88~108.20° in Mg-*cyclo*-N$_5^-$, respectively. The Δa_{max} values are 0.25 and 0.20° in Na-*cyclo*-N$_5^-$ and Mg-*cyclo*-N$_5^-$, respectively. These results indicate that *cyclo*-N$_5^-$ in these two crystals are distorted, and the distortion degree is higher in Na-

cyclo-N$_5^-$. Based on the optimized structure, the single point energy of *cyclo*-N$_5^-$ in the three species shown in Figure 2 is obtained by B3LYP with the basis set of 6-311++ G (d, p). Compared with the energy of undistorted *cyclo*-N$_5^-$, the ΔE values of Na-*cyclo*-N$_5^-$ and Mg-*cyclo*-N$_5^-$ are 0.35 and 0.33 kcal mol^{-1}, respectively. This means that the distortion does affect the stability of *cyclo*-N$_5^-$. The higher the degree of distortion of *cyclo*-N$_5^-$, the more unstable it is. However, due to the small difference in N−N BL and N−N−N angle between the two compounds, ΔE of *cyclo*-N$_5^-$ is not obvious. Therefore, the energy change caused by distortion of *cyclo*-N$_5^-$ is insignificant to the lattice energy and binding energy of the two crystal.

Furthermore, the detailed structural characteristics of *cyclo*-N$_5^-$ in these two samples were analyzed. In Na-*cyclo*-N$_5^-$, two N ↔ Na ion bonds and three O−H···N HBs are formed surrounding *cyclo*-N$_5^-$, as shown in Figure 2b. N1−N9 is the longest bond in *cyclo*-N$_5^-$ (red, 1.33 Å), while the other four N−N bonds are almost equal (black, 1.31 Å). Both N1 and N9 form Na ↔ N ion bonds with Na$^+$. The largest N−N−N angle is located at the para-position of the longest bond (N1−N9), which is 108.25°. In Mg-*cyclo*-N$_5^-$, the five N atoms of *cyclo*-N$_5^-$ form five O−H···N HBs, as shown in Figure 2c. N1−N4 is the longest bond in *cyclo*-N$_5^-$ (red, 1.32 Å), and both N1 and N4 form HBs with H$_2$O in [Mg(H$_2$O)$_6$]$^{2+}$. The largest N−N−N angle is located at the para-position of the longest bond (N1−N4), which is 108.20°. The distortion of *cyclo*-N$_5^-$ should be related to its stress in the crystal, which will be discussed later (Section 3.4).

3.2. Stability and Electronic Structures. As solid materials, the DOS and the band gap (BG) of an explosive crystal are frequently associated with stability: the narrower the BG is, the easier it is to excite the crystal and the less stable it is.[43,44] The total density of states (TDOS) of these two samples was calculated by the PBE functional. As seen in Figure 3, the BGs of Na-*cyclo*-N$_5^-$ and Mg-*cyclo*-N$_5^-$ are 4.33 and 5.15 eV, respectively. The BG of Mg-*cyclo*-N$_5^-$ is larger than that of Na-*cyclo*-N$_5^-$, implying that Mg-*cyclo*-N$_5^-$ is more stable, which is in good agreement with the results of lattice energy and binding energy calculations given above.

We further analyzed the contribution of metal ions and the surrounding bonding atoms near the valence bands and conduction bands in TDOSs. As shown in Figure 1a, Na1, N13, and O9 were selected as representatives, and their partial density of states (PDOS) values were calculated by PBE for comparative analysis. In Figure 3a, the s-orbital of O9 has a major contribution to the occupied state at −23.59 eV, and the s-orbital and p-orbital of N13 make a dominant contribution to the occupied state at −22.92 eV. The occupied states at −12.25 to −5 eV are mainly contributed by the s-orbital of Na1, the p-orbital of N13, and the p-orbital of O9. Among them, the s-orbital of Na1 and the p-orbital of N13 hybridize to form a coordination bond between *cyclo*-N$_5^-$ and Na-*cyclo*-N$_5^-$, sustaining its stability. The s-orbital of Na1 and the p-orbital of O9 hybridize to form a coordination bond between H$_2$O and Na. As shown in Figure 1c, Mg1 and O10 were selected as representatives, and their PDOS values were calculated by PBE
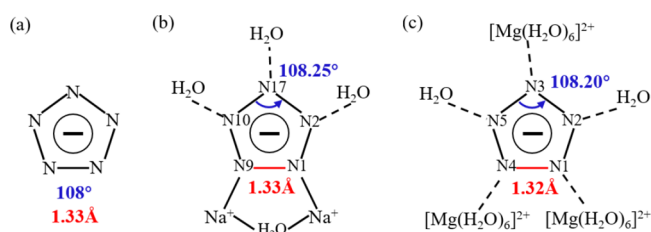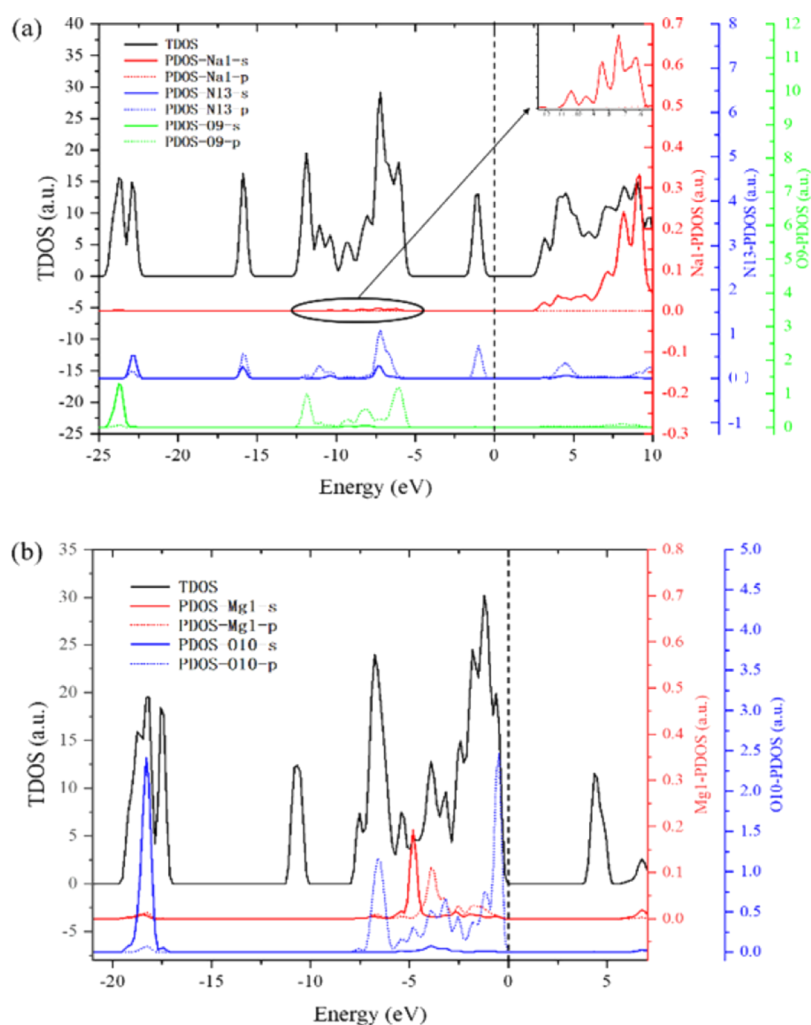
Figure 3. TDOS and PDOS calculated by PBE. (a) TDOS and PDOS of Na-*cyclo*-N_5^-: TDOS (black solid line); PDOS of Na1-s (red solid line); PDOS of Na1-p (red dotted line); PDOS of N13-s (blue solid line); PDOS of N13-p (blue dotted line); PDOS of O9-s (green solid line); and PDOS of O9-p (green dotted line). (b) TDOS and PDOS of Mg-*cyclo*-N_5^-: TDOS (black solid line); PDOS of Mg1-s (red solid line); PDOS of Mg1-p (red dotted line); PDOS of O10-s (blue solid line); and PDOS of O10-p (blue dotted line).

for comparative analysis. In Figure 3b, the occupied states between −7.5 and 0 eV are mainly contributed by the s-orbital and p-orbital of Mg1 and the p-orbital of O10. The s-orbital of Mg1 and the p-orbital of O10 are hybridized, resulting in the formation of a coordination bond between Mg and H_2O, maintaining the stability of the entire $[Mg(H_2O)_6]^{2+}$ structure. In Mg-*cyclo*-N_5^-, Mg^{2+} is not bonded with *cyclo*-N_5^-, so no hybridization occurs.

N ↔ Na ion bonds are formed between Na^+ and *cyclo*-N_5^- to sustain the stability of the crystal in Na-*cyclo*-N_5^-, while Mg does not bond with *cyclo*-N_5^- in Mg-*cyclo*-N_5^-. Logically, Na-*cyclo*-N_5^- should be more stable than Mg-*cyclo*-N_5^-. However, this conflicts with the result of BG calculations and energy calculations mentioned above. This indicates that the analysis of DOS does not articulate a clear reason why Mg-*cyclo*-N_5^- is more stable than Na-*cyclo*-N_5^-. For such novel EMs, in addition to the ion bonds, a weak interaction is also a very important factor affecting the stability of the crystal. Therefore, in order to get an in-depth analysis of the stability mechanism for these two samples, we focused on weak interactions.

3.3. Stability and Weak Interactions. *3.3.1. Hydrogen Bond.* In HEDMs, there are many weak interactions, such as HBs, van der Waals forces, and π-π stacking, in which HBs are

one of the important components and have great significance in sustaining the stability of the whole structure. A HB network was considered the main stabilization factor for the two nonmetallic *cyclo*-N_5^- energetic salts.[31] However, for such *cyclo*-N_5^- metal hydrates, systematic studies focusing on HBs have not previously been performed. As demonstrated in Figure 4, two types of HBs are contained in these two samples: O−H···O and O−H···N. In Na-*cyclo*-N_5^-, the distribution of HBs is relatively simple: O−H···N [signed as **a** in Figure 4a] on plane (100), O−H···O [signed as **b** in Figure 4a] on plane (100), and O−H···N [signed as **c** in Figure 4a] on plane (001). As shown in Figure 4a, **a** is located between free H_2O (*f*-H_2O) and *cyclo*-N_5^-, and its BL is approximately 1.88 Å. **b** is connected to the *f*-H_2O and the coordinated H_2O (*c*-H_2O), whose BL is approximately 1.74 Å. HB **c** is located between *c*-H_2O and *cyclo*-N_5^-, whose BL is approximately 1.94 Å. For *cyclo*-N_5^-, based on the above-mentioned PDOS analysis, it is known that the Na ↔ N ion bond is a factor in stabilizing *cyclo*-N_5^-. Moreover, the HBs **a** and **c** also stabilize *cyclo*-N_5^- in the crystal. For the whole crystal unit, HBs **a** and **b** make the *f*-H_2O stable, and HBs **c** sustain the stability between the upper and lower layers in the *b* axis. The details of the HB are listed in Table 4. Na-*cyclo*-N_5^- possess the face-to-face crystal packing (layer-by-layer crystal packing).
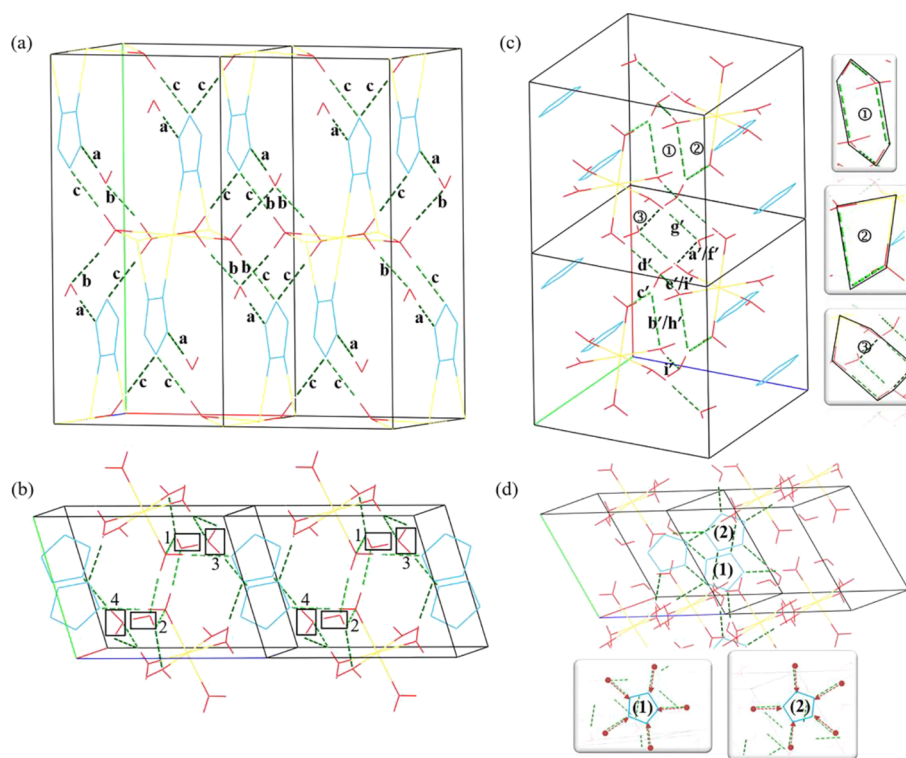
Figure 4. Wireframe models of HBs. (a) HBs in Na-*cyclo*-N$_5^-$. (b) HBs in Mg-*cyclo*-N$_5^-$. (c) O–H···O bonds in Mg-*cyclo*-N$_5^-$. (d) O–H···N bonds in Mg-*cyclo*-N$_5^-$. The *a*, *b*, and *c* directions in the unit cell axis are represented by red, green, and purple lines, respectively. The green dotted line indicates the HBs inside the model.

Both the intralayer 2D HB network (composed of HBs **a** and **b**) and the HBs between layers (HBs **c**) maintain the stability of the whole crystal.

In Mg-*cyclo*-N$_5^-$, the HBs are more complicated, as shown in Figure 4b–d. In Figure 4b, free H$_2$O 1 and 2 are located between the two [Mg(H$_2$O)$_6$]$^{2+}$ and far from *cyclo*-N$_5^-$, whose major role is to stabilize the two [Mg(H$_2$O)$_6$]$^{2+}$. We call them "free H$_2$O away from *cyclo*-N$_5^-$" (*fa*-H$_2$O). Free H$_2$O 3 and 4 are located between the [Mg(H$_2$O)$_6$]$^{2+}$ and *cyclo*-N$_5^-$, whose main function is to provide the interaction between *cyclo*-N$_5^-$ and [Mg-(H$_2$O)$_6$]$^{2+}$. We call them "free H$_2$O near *cyclo*-N$_5^-$" (*fn*-H$_2$O). Another class is the six H$_2$O molecules coordinated to Mg^{2+}. We call them "coordinated H$_2$O" (*c*-H$_2$O). All of these three types of water are involved in the formation of HBs. O–H···O bonds in Mg-*cyclo*-N$_5^-$ are shown in Figure 4c. There are five O–H···O bonds on each *fa*-H$_2$O, signed as **a′**, **b′**, **c′**, **d′**, and **e′**. The **a′** bond is composed of O–H in *fa*-H$_2$O and O in *fn*-H$_2$O, and its BL is approximately 1.66 Å. Bonds **b′** and **c′** are made up of O–H in *fa*-H$_2$O and O in *c*-H$_2$O, and their BLs are approximately 2.40 and 1.97 Å, respectively. The **d′** and **e′** bonds are built up by O–H in *c*-H$_2$O and O in *fa*-H$_2$O, and their BLs are approximately 1.707 and 1.67 Å, respectively. There are two O–H···O bonds for each *fn*-H$_2$O, which are labeled **f′** and **g′**. The O–H in *fa*-H$_2$O is connected to the O in *fn*-H$_2$O to form **f′**, which is equivalent to **a′**. Bond **g′** is between O in *fn*-H$_2$O and O–H in *c*-H$_2$O, whose BL is approximately 1.74 Å. Bonds **h′** and **i′** are the O–H···O bonds for *c*-H$_2$O, which are equivalent to **b′** and **e′**, respectively. In general, there are more O–H···O bonds in Mg-*cyclo*-N$_5^-$ than in Na-*cyclo*-N$_5^-$. These large numbers of HBs come together to form several ring structures, as shown in the small figures on the right side of Figure 4c. The details are shown in Table 5. The ring structures without Mg involvement

mainly sustain the stability of [Mg(H$_2$O)$_6$]$^{2+}$ in the model. The rings with Mg participation keep the free H$_2$O (both *fa*-H$_2$O and *fn*-H$_2$O) and [Mg(H$_2$O)$_6$]$^{2+}$ stable. The other type of HBs in Mg-*cyclo*-N$_5^-$, O–H···N bonds, are shown in Figure 4d. The unit cell contains two *cyclo*-N$_5^-$, which we labeled as (**1**) (N1, N2, N3, N4, and N5) and (**2**) (N6, N7, N8, N9, and N10). Every N on each *cyclo*-N$_5^-$ forms an O–H···N bond. In other words, 10 O–H···N bonds are formed in total. Among the N atoms, N2, N5, N7, and N10 form O–H···N bonds with *fn*-H$_2$O, and the others are formed with *c*-H$_2$O. There are no O–H···N bonds between *fa*-H$_2$O and *cyclo*-N$_5^-$. Therefore, *fn*-H$_2$O and *c*-H$_2$O play an important role in stabilizing *cyclo*-N$_5^-$.

The number of HBs in Mg-*cyclo*-N$_5^-$ is much greater than that in Na-*cyclo*-N$_5^-$: 3 HBs in the primitive cell of Na-*cyclo*-N$_5^-$ and 11 HBs in the primitive cell of Mg-*cyclo*-N$_5^-$.[24] Different from Na-*cyclo*-N$_5^-$ with a 2D HB network, these huge HBs in Mg-*cyclo*-N$_5^-$ (not only O–H···O bonds but also O–H···N bonds) form a strong 3D HB network. Moreover, many complex O–H···O ring microstructures are found in the 3D HB network. This means the 3D HB network is superior to the 2D HB network in improving stability. After analyzing the specific structure of the HBs in these two samples, we will further reveal the stability mechanism from the strength of the HB and other weak interactions.

We employed Hirshfeld surfaces to show the weak interactions in these two samples. These surfaces refer to the isosurface of a ratio of the atomic electron density in a particular molecule to the atomic electron density sum of all molecules in the crystal of 0.5. The strength and direction of the interactions in the crystal can be described using the standardized contact distance d_{norm} (normalized contact distance). d_{norm} can be obtained according to the following formula 3, where d_i and d_e

Table 4. Summary of Hydrogen Bonding Interactions (D−H···R; Å) Operating in the Crystal Structures of Na-*Cyclo*-N$_5^-$ and Mg-*Cyclo*-N$_5^{-a}$

donor	H	receptor	D−H (Å)	H···R (Å)	symmetry op.
			Na-*cyclo*-N$_5^-$		
O1	H17	N4	0.99	1.88	x, y, z; $-1 + x, y, z$
O1	H21	N12	0.99	1.88	x, y, z; x, y, z
O2	H18	N2	0.99	1.88	x, y, z; $x, 1 + y, z$
O2	H22	N10	0.99	1.88	x, y, z; $1 + x, 1 + y, z$
O3	H19	N8	0.99	1.88	x, y, z; $x, -1 + y, z$
O3	H23	N16	0.99	1.88	$x, y, 1 + z$; $-1 + x, -1 + y, z$
O4	H20	N6	0.99	1.88	x, y, z; $1 + x, y, z$
O4	H24	N14	0.99	1.88	$x, y, 1 + z$; x, y, z
O5	H1	O1	1.00	1.73	x, y, z; x, y, z
O5	H2	N20	0.98	1.94	x, y, z; $x, y, -1 + z$
O6	H3	O2	1.00	1.73	x, y, z; x, y, z
O6	H4	N19	0.98	1.94	x, y, z; $1 + x, 1 + y, -1 + z$
O7	H5	O3	1.00	1.73	x, y, z; x, y, z
O7	H6	N18	0.98	1.94	x, y, z; $-1 + x, -1 + y, z$
O8	H7	O4	1.00	1.73	x, y, z; x, y, z
O8	H8	N17	0.98	1.94	x, y, z; x, y, z
O9	H9	O1	1.00	1.73	x, y, z; x, y, z
O9	H10	N20	0.98	1.94	x, y, z; $x, y, -1 + z$
O10	H11	O2	1.00	1.74	x, y, z; x, y, z
O10	H12	N19	0.98	1.94	x, y, z; $1 + x, 1 + y, -1 + z$
O11	H13	O3	1.00	1.74	x, y, z; $x, y, -1 + z$
O11	H14	N18	0.98	1.94	x, y, z; $-1 + x, -1 + y, -1 + z$
O12	H15	O4	1.00	1.74	x, y, z; $x, y, -1 + z$
O12	H16	N17	0.98	1.94	x, y, z; $x, y, -1 + z$
			Mg-*cyclo*-N$_5^-$		
O1	H2	N8	0.99	1.88	x, y, z; x, y, z
O1	H1	O3	1.00	1.67	x, y, z; ; $-1 + x, -1 + y, z$
O2	H8	N5	0.99	1.81	x, y, z; $1 + x, y, 1 + z$
O2	H9	N2	0.99	1.86	x, y, z; $1 + x, 1 + y, 1 + z$
O3	H7	O10	0.99	2.40	x, y, z; $1 + x, 1 + y, 1 + z$
O3	H7	O6	0.99	1.97	x, y, z; $1 + x, 1 + y, 1 + z$
O3	H6	O2	1.01	1.66	x, y, z; x, y, z
O4	H3	N4	0.99	1.85	x, y, z; $x, -1 + y, z$
O4	H4	O7	1.00	1.74	x, y, z; $2 + x, 1 + y, 1 + z$
O5	H5	O3	1.00	1.71	x, y, z; x, y, z
O5	H10	N1	0.99	1.84	x, y, z; x, y, z
O6	H11	O8	1.00	1.67	x, y, z; $1 + x, 1 + y, z$
O6	H12	N3	0.99	1.88	x, y, z; x, y, z
O7	H18	N10	0.99	1.81	x, y, z; $-1 + x, y, -1 + z$
O7	H19	N7	0.99	1.86	x, y, z; $-1 + x, -1 + y, -1 + z$
O8	H16	O7	1.01	1.66	x, y, z; x, y, z
O8	H17	O1	0.99	1.97	x, y, z; $-1 + x, -1 + y, -1 + z$
O8	H17	O5	0.99	2.40	x, y, z; $-1 + x, -1 + y, -1 + z$
O9	H13	N9	0.99	1.85	x, y, z; $x, 1 + y, z$
O9	H14	O2	0.99	1.74	x, y, z; $-2 + x, -1 + y, -1 + z$
O10	H15	O8	1.00	1.71	x, y, z; x, y, z
O10	H20	N6	0.99	1.84	x, y, z; x, y, z

^{a}The distance of H···R and the angle of D−H···R are limited to shorter than 2.5 Å and larger than 120°, respectively.

Table 5. Ring Structure Related to O−H···O Bonds in Mg-*cyclo*-N$_5^-$ Corresponding to Figure 4c

	type of rings	type of H$_2$O involved	HB involved (Å)	
no Mg participation	① O−H···O− H···O−H··· O−H···O	two *fa*-H$_2$O; two *c*-H$_2$O	**b′/h′**	2.40
			e′/i′	1.67
Mg participation	② Mg−O−H··· O−H···O− H−O−Mg	one *fa*-H$_2$O; one *fn*-H$_2$O; two *c*-H$_2$O and one Mg	**a′/f′**	1.66
			d′	1.71
			g′	1.74
	③ Mg−O···H··· O−Mg	one *fa*-H$_2$O; two *c*-H$_2$O; and one Mg	**b′/h′**	2.40
			c′	1.97

Waals radii of the corresponding atom in-plane and out-of-plane (Å), respectively.[45−48]

$$d_{norm} = \frac{d_i - r_i^{vdW}}{r_i^{vdW}} + \frac{d_e - r_e^{vdW}}{r_e^{vdW}} \tag{3}$$

d_{norm} enables the identification of regions of particular importance to interactions. That is, a Hirshfeld surface is composed of many points, and each point parameterized as (d_i, d_e) can provide information about the related contact distances from it. A relatively low $d_i + d_e$ suggests close atom−atom contact. Mapping these (d_i, d_e) points and considering their relative frequencies, one can obtain a 2D fingerprint plot. The color mapping distinguishes the intensities and distances of points.[49] All the surfaces and fingerprint plots were created using CrystalExplorer 3.1.

To study the stability and weak interactions of these two samples more effectively, we selected different parts for Hirshfeld surface analysis. For Na-*cyclo*-N$_5^-$, we selected three Na$^+$ in the middle of the model, which paralleled to the *c*-axis, two *cyclo*-N$_5^-$ bonded to the center Na$^+$, and four *c*-H$_2$O molecules surrounding the center Na$^+$ to create the surface, totally 25 atoms. For Mg-*cyclo*-N$_5^-$, we chose one [Mg-(H$_2$O)$_6$]$^{2+}$ structure to create the surface. In Figure 5, we performed three different types of surfaces: Hirshfeld, shape index, and curvedness surfaces. When analyzing the Hirshfeld surfaces, we focused on the red part of the surface, where the interaction between the molecules is the strongest, and the interactions represented by white and blue are progressively weaker than those shown by red. The shape index is a qualitative measure of shape and can be sensitive to very subtle changes in surface shape, particularly in regions where the total curvature (or the curvedness) is very low. The shape index shows a red concave region on the surface around the acceptor atom and a blue region around the donor H atom.[50] Curvedness is a function of the root-mean-square curvature of the surface, and maps of curvedness typically show large, green (relatively flat) regions separated by dark blue edges (large positive curvature).

In Na-*cyclo*-N$_5^-$, as demonstrated in Figure 5a, the interactions are mainly concentrated on three atoms of N, H, and O, including H···N, H···O, and H···H. The upper and lower layers along the *b* axis are not directly connected with coordination bonds but form a stable structure by H···N interaction (marked with 1 in Figure 5a), that is, HB **c** in Figure 4a. Along the *c*-axis, H···N interactions (marked with 3 in Figure 5a) are formed, that is, HB **a** in Figure 4a. H···O intermolecular interactions (marked with 2 in Figure 5a) are formed between H in *c*-H$_2$O and O in *f*-H$_2$O, that is, HB **b** in Figure 4a. It can be seen from the shape index diagram that in the H···N interactions (marked with 1′ and 3′ in Figure 5a, corresponding to the
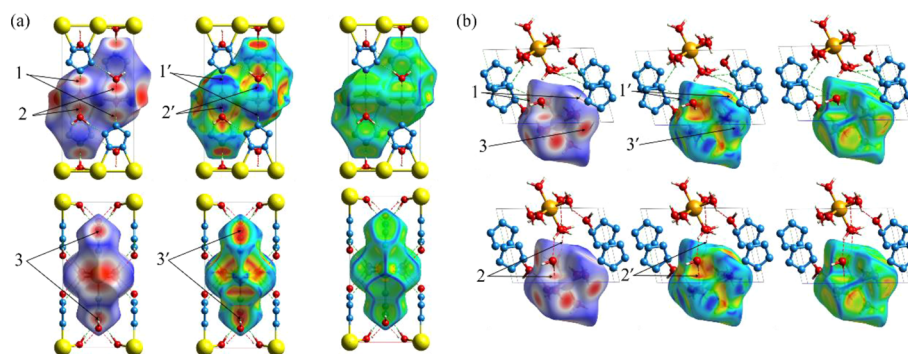
represent the distance from the point on the Hirshfeld surface to the nearest atom in the in-plane and out-of-plane (Å), respectively. In addition, r_i^{vdW} and r_e^{vdW} represent the van der

Figure 5. Hirshfeld surfaces of Na-*cyclo*-N_5^- and Mg-*cyclo*-N_5^- and with a variety of properties mapped onto the surface. (a, b) Na-*cyclo*-N_5^- and Mg-*cyclo*-N_5^-, respectively. H···N is shown in a green dotted line. H···O is shown in a red dotted line. The first row: Hirshfeld surfaces, mapped on its natural range (i.e., from minimum to maximum) of −0.668/−0.707 (red) to +1.153/+1.356 a.u.$^{-1}$ (blue); the second row: shape index, mapped from −1.0 /−0.992 (concave umbilic; red), 0.150/+0.376 (minimal saddle; green), and +0.998/+0.998 (convex umbilic; blue); the third row: curvedness, C, mapped from −3.264/−0.407 (flat; red), −0.981/−0.957 (unit sphere; cyan−green), and +0.448/+0.338 (edge; blue).
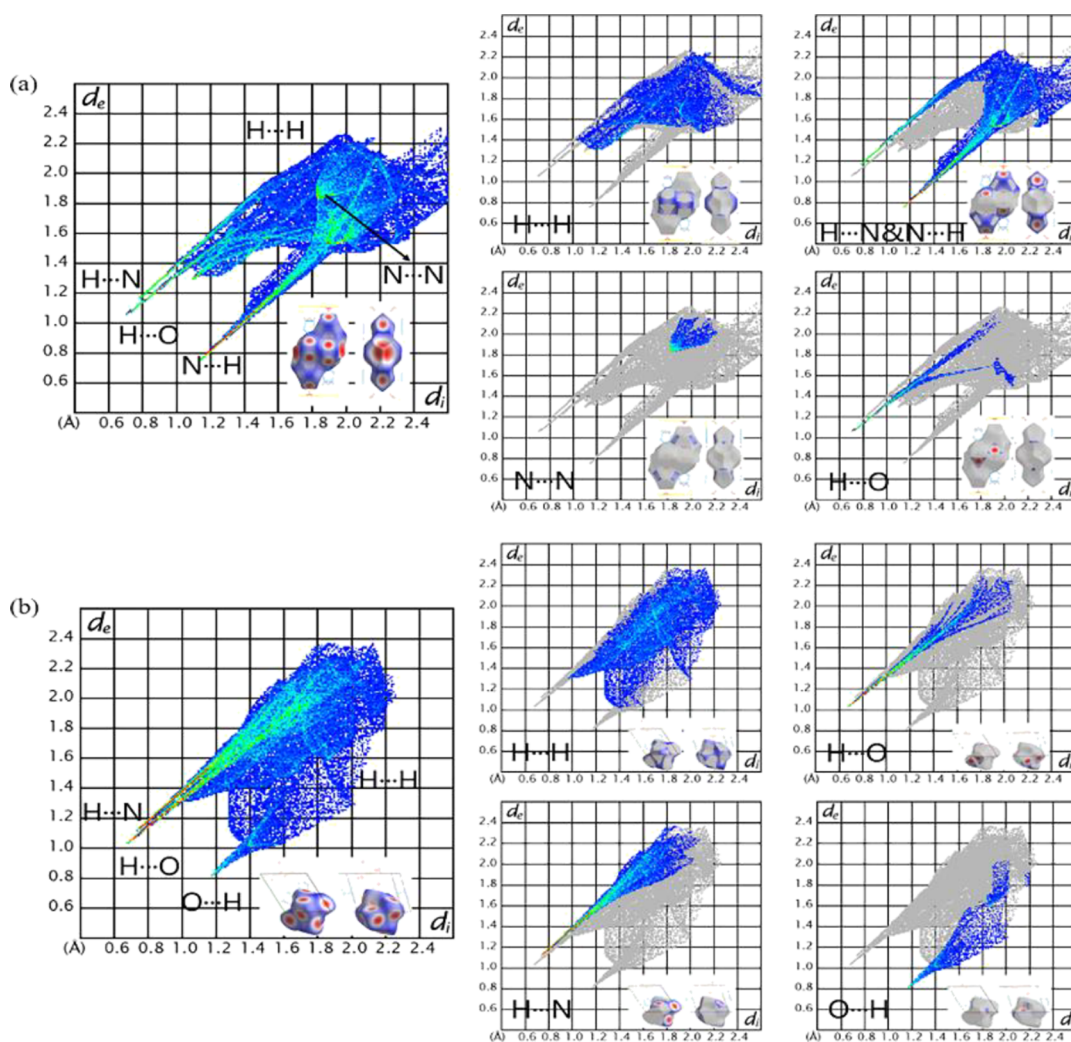

Figure 6. 2D fingerprint plots of corresponding to Figure 5. (a) Left: 2D fingerprint plots of Na-*cyclo*-N_5^-. Right: 2D fingerprint plots mapped by elements. Bottom right corner: Hirshfeld surfaces corresponding to the interaction. (b) Left: 2D fingerprint plots of Mg-*cyclo*-N_5^-. Right: 2D fingerprint plots mapped by elements. Bottom right corner: Hirshfeld surfaces corresponding to the interaction. A···B: A represents an atom inside the surfaces, and B represents an atom outside the surface.

preceding 1 and 3), when H is outside the surface, the surface appears red (concave), and when H is located inside the surface, the surface appears blue (convex). This implies that the H atoms in the H···N interactions are donor atoms. Similarly, the donor

atoms in the H···O bonds (marked with 2′ in Figure 5a, corresponding to the preceding 2) are also H atoms. Overall, there are two kinds of interactions in Na-*cyclo*-N_5^-; one is the electrostatic interaction between *cyclo*-$N_5^-$and H_2O, and the

other is the intermolecular interaction between c-H_2O and f-H_2O. The curvature diagram is almost green, indicating that the curvature is relatively small and the surface is relatively flat.

In Mg-$cyclo$-N_5^-, as shown in Figure 5b, the type of interaction is similar to that shown in Figure 5a. $cyclo$-N_5^- is stabilized by H⋯N interactions (marked with 1 in Figure 5b), that is, HBs related to $cyclo$-N_5^- in Figure 4d. The upper and lower $[Mg(H_2O)_6]^{2+}$ ions along the b axis form a stable structure by H⋯O interactions (marked with 2 in Figure 5b), that is, HBs a′, b′, c′, d′, e′, f′, h′, and i′ in Figure 4c. Two fn-H_2O molecules located on the diagonal of the model also formed H⋯O interactions (marked with 3 in Figure 5b)] with c-H_2O, that is, HB g′ in Figure 4c. Similar to Figure 5a, the donor atoms in the H⋯N (marked with 1′ in Figure 5b, corresponding to the preceding 1) and H⋯O (marked with 2′ and 3′ in Figure 5b, corresponding to the preceding 2 and 3) are H atoms. There are also two kinds of interactions in Mg-$cyclo$-N_5^-; one is the electrostatic interaction between $cyclo$-N_5^- and H_2O, and the other is the intermolecular interaction among the three types of H_2O molecules. Not only is there no bond between $cyclo$-N_5^- and Mg^{2+}, but also there is no interaction. The curvature diagram shows the amount of red and yellow areas, indicating that the surface curvature is relatively large. This suggests that a large curvature may contribute to the production of interactions, which in turn increases the ratio of intermolecular/electrostatic interactions in the model and thereby enhances the stability of the crystal. Compared to Na-$cyclo$-N_5^-, Mg-$cyclo$-N_5^- has more coordination H_2O and free H_2O, which increases the complexity of its intermolecular and electrostatic interactions.

From the Hirshfeld surface, we can further obtain the 2D fingerprint to analyze the strength of the interaction. When performing 2D fingerprint analysis, two points are generally considered. One is the point of min $(d_i + d_e)$, which is located in the bottom-left corner of a fingerprint plot and accompanied by sharp peaks. The smaller the min $(d_i + d_e)$, the higher the interaction strength. The other is the frequency at which the point appears: red means that there are many points in the area, and green and blue indicate a successive decreasing number of points. Figure 6 shows the 2D fingerprint plots of these two models. To observe the proportion of each type of interaction directly, Figure 7 shows the percentage chart of contact populations.

In Na-$cyclo$-N_5^-, as shown in Figure 6a, there are three sharp peaks in the bottom-left corner: H⋯N (green), H⋯O (green)

and N⋯H (red). As analysis above, weak interaction H⋯N and N⋯H are both O−H⋯N HBs, and weak interaction H⋯O is O−H⋯O HB. Therefore, in Na-$cyclo$-N_5^-, HB is the strongest interaction. The min $(d_i + d_e)$ of N⋯H is approximately 1.9 Å, whereas the min $(d_i + d_e)$ of H⋯O is approximately 1.8 Å. Therefore, in Na-$cyclo$-N_5^-, the strength of O−H⋯O is stronger than O−H⋯N. The red peak of N⋯H indicates that it possesses a higher frequency. As shown in Figure 7, the proportions of N⋯H, H⋯O, and H⋯H are 50.6, 7.9, and 21.9%, respectively. Meanwhile, in Mg-$cyclo$-N_5^-, there are three sharp peaks in the bottom-left corner: H⋯N (red), H⋯O (red), and O⋯H (blue), as shown in Figure 6b. The min $(d_i + d_e)$ of N⋯H is approximately 1.8 Å, whereas the min $(d_i + d_e)$ of H⋯O is approximately 1.7 Å. As a result, the strength of O−H⋯O is stronger than O−H⋯N in Mg-$cyclo$-N_5^-. Red peaks of N⋯H and H⋯O indicate that their frequencies are relatively high. As shown in Figure 7, the proportions of N⋯H, H⋯O, and H⋯H are 32.1, 27.8, and 39.9%, respectively. They also play a role in stability.

According to the results of Hirshfeld surfaces and 2D fingerprint, O−H⋯O and O−H⋯N are the strongest interactions in both the samples, which play a major role in maintaining the stability of the crystal. The strength of O−H⋯O is higher than that of O−H⋯N. Therefore, O−H⋯O has a higher contribution to sustaining the stability of the whole crystal. Because the HBs around $cyclo$-N_5^- in both samples are all O−H⋯N, they stabilize $cyclo$-N_5^- in the crystal. In Table 4, the distance of H⋯O and H⋯N is shorter in Mg-$cyclo$-N_5^- than in Na-$cyclo$-N_5^-, which indicates that the HBs in Mg-$cyclo$-N_5^- may be stronger. This inference is verified here. Comparing the min $(d_i + d_e)$ of two samples, the strength of O−H⋯O and O−H⋯N in Mg-$cyclo$-N_5^- is slightly higher than that in Na-$cyclo$-N_5^-. This is another reason why Mg-$cyclo$-N_5^- is more stable.

3.3.2. π-π Stacking Interaction. Moreover, because the Hirshfeld surface group we selected above is $[Mg(H_2O)_6]^{2+}$ in Mg-$cyclo$-N_5^-, N was not selected. Therefore, the interaction force between N⋯N in Mg-$cyclo$-N_5^- was not considered, which we will discuss further below. As shown in the lower left corner of Figure 8a, we selected one $cyclo$-N_5^- (N1−N2−N3−N4−N5) to perform the Hirshfeld surface and 2D fingerprint plot. The N⋯N interaction accounts for 16.4% of interactions, and the other proportion was contributed by the N⋯H interaction. Therefore, in addition to O−H⋯N, N⋯N also plays an important role in sustaining the stability of $cyclo$-N_5^- in Mg-$cyclo$-N_5^-. As demonstrated in Figure 8b, N⋯N interactions mean that there are face-to-face π-π stacking interactions in the two parallel $cyclo$-N_5^-. The distance between two $cyclo$-N_5^- is 3.29 Å, which is shorter than the distance between $cyclo$-N_5^- in $[Ag(NH_3)_2]^+[Ag_3(N_5)_4]^-$ (3.84 and 3.63 Å).[27] Therefore, the strength of π-π stacking interactions in Mg-$cyclo$-N_5^- is even stronger than that in $[Ag(NH_3)_2]^+[Ag_3(N_5)_4]^-$. Although there are N⋯N interactions in Na-$cyclo$-N_5^- (Figures 6 and 7), there are no face-to-face π-π stacking interactions between $cyclo$-N_5^- according our calculations. When the centroid−centroid distance is less than 3.80 Å, and the angle between the centroid−centroid line and vertical line is less than 20°, face-to-face π-π stacking interactions will exist.[51] The centroid−centroid distance in Na-$cyclo$-N_5^- is 4.924 Å and the angle between centroid−centroid line and vertical line is approximately 45°. The abovementioned conditions are not satisfied, so there is no face-to-face π-π stacking interaction between two parallel $cyclo$-N_5^- in Na-$cyclo$-N_5^-. The N⋯N in Na-$cyclo$-N_5^- is
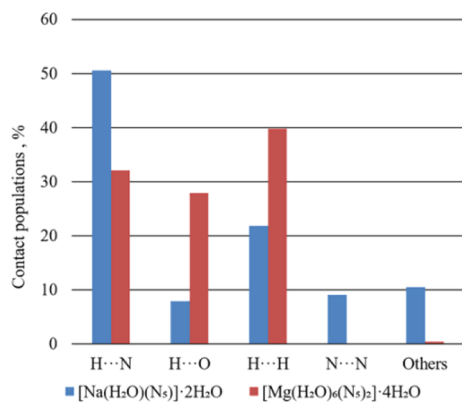

Figure 7. Distribution of individual intermolecular interactions on the basis of Hirshfeld surface analysis of Na-$cyclo$-N_5^- and Mg-$cyclo$-N_5^-. A⋯B: include reciprocal contacts.
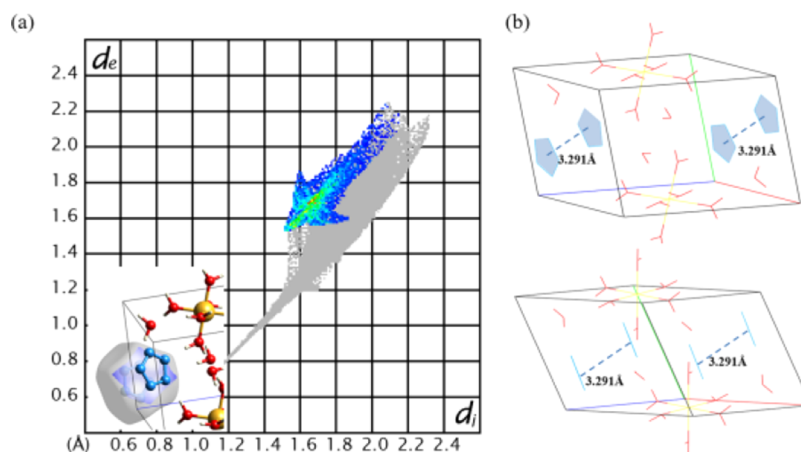
Figure 8. N···N interaction in Mg-*cyclo*-N_5^-. (a) 2D fingerprint plots of N···N. In the lower left corner is the corresponding Hirshfeld surface. (b) Structure of two *cyclo*-N_5^-. The *a*, *b*, and *c* directions in the unit cell axis are represented by red, green, and purple lines, respectively. The blue dotted line indicates the distance between two *cyclo*-N_5^-.
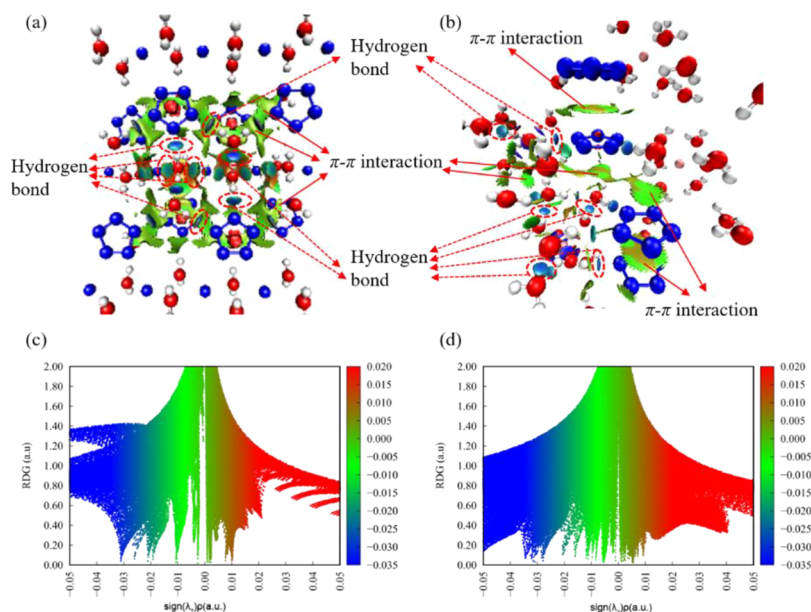

Figure 9. Noncovalent interaction analyses. (a, b) Color-filled reduced density gradient (RDG) isosurface for Na-*cyclo*-N_5^- and Mg-*cyclo*-N_5^-, respectively. (c, d) Scatter graphs for Na-*cyclo*-N_5^- and Mg-*cyclo*-N_5^-, respectively. Blue: strong attraction; green: weak interaction; red: strong repulsion.

just the edge-to-edge weak interaction between two adjacent *cyclo*-N_5^- rings.

To get the scope of weak interaction intuitively, noncovalent interaction analysis was performed by Multiwfn,[53] and the results are shown in Figure 9. From the color-filled reduced density gradient (RDG) isosurface,[54] we can identify different types of regions by simply examining their colors. The dark blue implies the stronger attractive interaction, which is considered to be hydrogen bonding. The green can be identified as the vdW interaction region, which exhibits that the density electron in this region is low. The red means the strong repulsion. In Figure 9a,b, it can be seen that the elliptical slab between between nitrogen atoms from *cyclo*-N_5^- and hydrogen atoms from H_2O shows blue color, so we can conclude that there is a HB. From their scatter graphs (Figure 9c,d), it can be found that the HBs in Mg-*cyclo*-N_5^- are stronger than those in Na-*cyclo*-N_5^-, which is consistent with the Hirshfeld surface analysis in Figure 6. Obviously, the regions at the center of the *cyclo*-N_5^- rings

correspond to a strong steric interaction because they are filled by red. From both RDG isosurface and scatter graphs, the *π*-*π* interaction regions in Mg-*cyclo*-N_5^- are significantly larger than those in Na-*cyclo*-N_5^-. Although Na-*cyclo*-N_5^- is a layer-by-layer crystal packing structure, the interlayer *π*-*π* interaction is discontinuous, due to the misalignment of the *cyclo*-N_5^- ring between layers by approximately 45°. Just the small-area edge-to-edge *π*-*π* interaction between two adjacent *cyclo*-N_5^- rings was observed. However, Mg-*cyclo*-N_5^- has large areas of face-to-face *π*-*π* interactions between two parallel *cyclo*-N_5^- rings. Therefore, *π*-*π* stacking interactions between two *cyclo*-N_5^- also play an important role in sustaining stability for these two samples. Our analysis shows that it is stronger in Mg-*cyclo*-N_5^- than that in Na-*cyclo*-N_5^-. It is also one reason why Mg-*cyclo*-N_5^- is more stable than Na-*cyclo*-N_5^-.

For these two samples, there are two main noncovalent interactions in the crystals: HB and *π*-*π* interaction. According to Figure 9, the more negative the sign(λ_2)ρ, the higher the
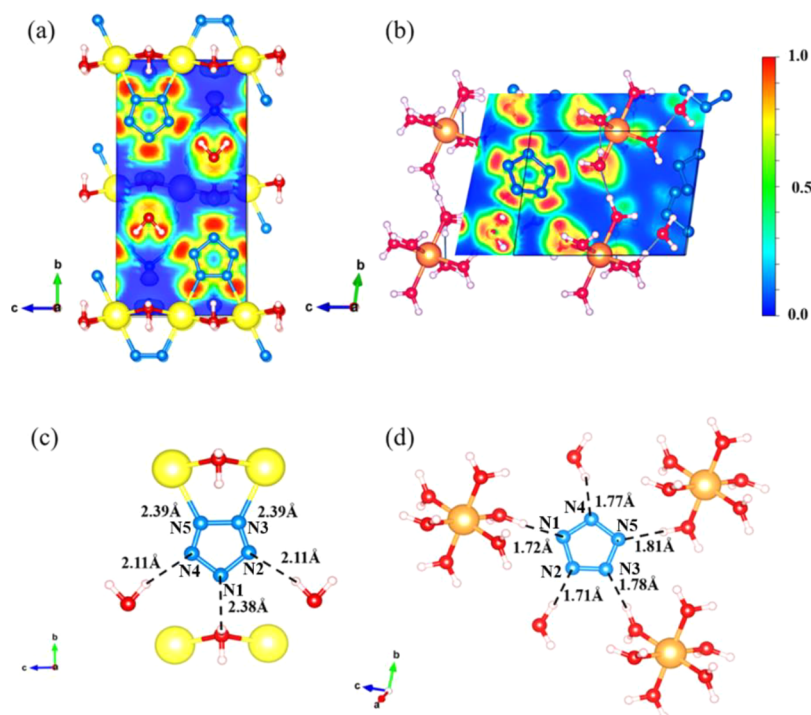
Figure 10. Interactions around *cyclo*-N_5^-, bond length, and ELF calculated on the *cyclo*-N_5^- plane. (a, b) ELF of Na-*cyclo*-N_5^- and Mg-*cyclo*-N_5^-, respectively (c, d) Interactions around *cyclo*-N_5^-: black dotted line indicates the distance of interaction.

strength of the interaction. It is clear that the strength of HB is much higher than that of π-π interaction. Therefore, HB is the most important factor of the stabilization mechanism. O−H···O is stronger and can stabilize the crystal, while O−H···N is connected with N in *cyclo*-N_5^-, so it mainly stabilizes *cyclo*-N_5^-. Both 2D and 3D HB networks stabilize the crystal structure. The nature of HB in the crystal is electrostatic interaction (blue), while the nature of π-π interaction is dispersion, and its strength is lower than that of HB. Face-to-face π-π interaction only exists in Mg-*cyclo*-N_5^- and mainly stabilizes the *cyclo*-N_5^- ring. Other types of π-π interaction contribute to the stability of the crystal.

3.4. Stability and *Cyclo*-N_5^-. To further analyze the stability mechanism of *cyclo*-N_5^- in the crystal, we calculated the electron localization function (ELF) of the *cyclo*-N_5^- plane, as shown in Figure 10. The ELF represents the relative degree of electron localization in the periodic structures.[52] According to the definition, $0 \leq$ ELF ≤ 1, the closer the ELF value is to 1, the higher the degree of electron localization (red area); in the area close to 0.5, electrons have the property of free electrons (green area); in the area close to 0, there is almost no electron localization (blue area). In Figure 10a, the electrons around *cyclo*-N_5^- are mainly concentrated on the N ↔ Na ion bond and O−H···N. Among them, the red area of N ↔ Na is relatively large, which indicates that the force is relatively strong, and the O−H···N interaction is obviously weaker than that of N ↔ Na. The different bonding modes surrounding *cyclo*-N_5^-, ion bond, and HB result in the nonuniform stress of *cyclo*-N_5^- in Na-*cyclo*-N_5^-. As analyzed in Figure 2b, the distortion of *cyclo*-N_5^- is caused by such nonuniform stress. *Cyclo*-N_5^- will be more likely to decompose into N_2 and N_3^- upon stimulation. As reported for $[M(N_5)_2(H_2O)_4]\cdot 4H_2O$ (M = Mn, Fe, Co, and Zn), *c*-H_2O binds with M to reduce the M ↔ *cyclo*-N_5^- interaction, leading to a less activated *cyclo*-N_5^- and higher kinetic barriers for its decomposition.[6] It is suggested that the formation of the Metal-N (Na ↔ N) ion bond is not beneficial to the stability of *cyclo*-

N_5^- when the metal cation (Na^+) acts as *cyclo*-N_5^- trap. In Figure 10b, the force around *cyclo*-N_5^- is relatively uniform, resulting in a lower *cyclo*-N_5^- distortion (as shown in Figure 2c and Table 3) and, in turn, increased stability. All five uniformly stressed HBs take advantage of their permanent electrostatic interaction with *cyclo*-N_5^- to inhibit decomposition. In Figure 10c,d, the distance between N···H in Mg-*cyclo*-N_5^- is approximately 0.44 Å shorter than that in Na-*cyclo*-N_5^-. Therefore, the N···H interaction in Mg-*cyclo*-N_5^- is stronger, which is consistent with the Hirshfeld and 2D fingerprint analysis.

In Table 6, the Laplacian bond order (LBO) of *cyclo*-N_5^- in the two species was calculated by Multiwfn.[53] LBO is adopted to

Table 6. Laplacian Bond Order (LBO) of *Cyclo*-N_5^- in Na-*Cyclo*-N_5^- and Mg-*Cyclo*-N_5^- Corresponding to Figure 10c,d, Respectively

	bond	LBO
Na-*cyclo*-N_5^-	N1−N2	1.50
	N1−N4	1.50
	N2−N3	1.42
	N4−N5	1.42
	N3−N5	1.52
Mg-*cyclo*-N_5^-	N1−N2	1.52
	N1−N4	1.53
	N2−N3	1.46
	N4−N5	1.45
	N3−N5	1.55

judge the strength of bond covalency, which is based on integrating negative parts of Laplacian of electron density in fuzzy overlap space.[55] LBO has a direct correlation with the bond polarity, the bond dissociation energy, and the bond vibrational frequency. In Na-*cyclo*-N_5^-, LBOs of N2-N3 and N4-

N5 are the smallest, both of which are 1.42. Compared with the other three N−N bonds in the $cyclo\text{-}N_5^-$, their bond covalency is lower, so their strength is the lowest. This is consistent with the results of the ELF analysis mentioned above. The force on N3 and N5 is the strongest, so $cyclo\text{-}N_5^-$ is easy to break at the position of N2−N3 and N4−N5 to form N_2 and N_3^- under high temperature and high pressure. In $Mg\text{-}cyclo\text{-}N_5^-$, the weakest LBO is N4−N5, 1.45, followed by N2−N3, 1.46. Their bond covalency is stronger than $cyclo\text{-}N_5^-$ in $Na\text{-}cyclo\text{-}N_5^-$. The covalency difference of the five N−N bonds in $cyclo\text{-}N_5^-$ of $Mg\text{-}cyclo\text{-}N_5^-$ is smaller than that of Na- $cyclo\text{-}N_5^-$. Therefore, $cyclo\text{-}N_5^-$ is more stable in $Mg\text{-}cyclo\text{-}N_5^-$ than in $Na\text{-}cyclo\text{-}N_5^-$. This further proves that $Mg\text{-}cyclo\text{-}N_5^-$ is more stable, consistent with the abovementioned analysis results.

4. CONCLUSIONS

Stability has always been an important topic in the study of $cyclo\text{-}N_5^-$-containing HEDMs. In this work, we gained insights into the factors affecting the stability of $Na\text{-}cyclo\text{-}N_5^-$ and $Mg\text{-}cyclo\text{-}N_5^-$ HEDMs by the first-principles method. Both binding/lattice energy calculations and DOS analysis show that $Mg\text{-}cyclo\text{-}N_5^-$ is more stable than $Na\text{-}cyclo\text{-}N_5^-$.

For these two samples, two types of HBs, O−H···O and O−H···N, are the main factors in the stabilization mechanism. The O−H···O is stronger and can stabilize the crystal, while O−H···N is connected with N in $cyclo\text{-}N_5^-$, so it mainly stabilizes $cyclo\text{-}N_5^-$.

For the crystal, the intralayer 2D HB network in $Na\text{-}cyclo\text{-}N_5^-$ and the 3D HB network in $Mg\text{-}cyclo\text{-}N_5^-$ are formed. Many complex O−H···O ring microstructures, the huge number of HBs, and the larger Hirshfeld surface curvature of metal cation groups are found in the 3D HB network. For such reasons, the 3D HB network is considered superior to the 2D HB network.

For $cyclo\text{-}N_5^-$, in addition to O−H···N HBs, π-π stacking interaction is also an important stabilizing factor. Nonuniform stress caused by different bonding modes results in the distortion of $cyclo\text{-}N_5^-$. Two N ↔ Na ion bonds and three HBs are formed surrounding $cyclo\text{-}N_5^-$ in $Na\text{-}cyclo\text{-}N_5^-$, while $cyclo\text{-}N_5^-$ in $Mg\text{-}cyclo\text{-}N_5^-$ is not bonded with metal ions Mg^{2+}, but five HBs are formed. ELF analysis shows the nonuniform stress on $cyclo\text{-}N_5^-$ in $Na\text{-}cyclo\text{-}N_5^-$. Comparing the two samples, the distortion degree of $cyclo\text{-}N_5^-$ is higher in $Na\text{-}cyclo\text{-}N_5^-$, which may more likely induce $cyclo\text{-}N_5^-$ decomposition. Maintaining the uniform stress of $cyclo\text{-}N_5^-$ is crucial to reduce its distortion.

In summary, our findings not only reveal the stabilization mechanism of two $cyclo\text{-}N_5^-$-containing metal hydrates, but also enhance the prospects for the design and synthesis of such novel $cyclo\text{-}N_5^-$-containing HEDMs.

■ AUTHOR INFORMATION

Corresponding Authors

Pengfei Lu − *State Key Laboratory of Information Photonics and Optical Communications, Ministry of Education, Beijing University of Posts and Telecommunications, Beijing 100876, China*; Email: photon.bupt@gamil.com

Jun Chen − *Beijing Applied Physics and Computational Mathematics, Beijing 100088, China*; Email: jun_chen@iapcm.ac.cn

Authors

Xiang Li − *School of Science and State Key Laboratory of Information Photonics and Optical Communications, Ministry of Education, Beijing University of Posts and Telecommunications, Beijing 100876, China; Beijing Applied Physics and Computational Mathematics, Beijing 100088, China*; orcid.org/0000-0003-3840-6500

Yao Long − *Beijing Applied Physics and Computational Mathematics, Beijing 100088, China*; orcid.org/0000-0002-7383-8109

Chong Zhang − *School of Chemical Engineering, Nanjing University of Science and Technology, Nanjing, Jiangsu 210094, China*

Chengguo Sun − *School of Chemical Engineering, University of Science and Technology Liaoning, Anshan, Liaoning 114051, China*; orcid.org/0000-0003-3580-2153

Bingcheng Hu − *School of Chemical Engineering, Nanjing University of Science and Technology, Nanjing, Jiangsu 210094, China*; orcid.org/0000-0002-0371-8128

Complete contact information is available at:
https://pubs.acs.org/10.1021/acsomega.1c05961

Notes

The authors declare no competing financial interest.

■ ACKNOWLEDGMENTS

■ REFERENCES

(1) Glukhovtsev, M. N.; Jiao, H.; Schleyer, P. R. Besides N_2, What Is the Most Stable Molecule Composed Only of Nitrogen Atoms? *Inorg. Chem.* **1996**, *35*, 7124−7133.

(2) Christe, K. O. Recent Advances in the Chemistry of N_5^+, N_5^- and High-Oxygen Compounds. *Propellants Explos. Pyrotech.* **2007**, *32*, 194−204.

(3) Singh, R. P.; Verma, R. D.; Meshri, D. T.; Shreeve, J. M. Energetic nitrogen-rich Salts and Ionic Liquids. *Angew. Chem., Int. Ed.* **2006**, *45*, 3584−3601.

(4) Wang, P.; Xu, Y.; Lin, Q.; Lu, M. Recent advances in the syntheses and properties of polynitrogen pentazolate anion $cyclo\text{-}N5^-$ and its derivatives. *Chem. Soc. Rev.* **2018**, *47*, 7522−7538.

(5) Hirshberg, B.; Gerber, R. B.; Krylov, A. I. Calculations predict a stable molecular crystal of N_8. *Inorg. Chem.* **2014**, *6*, 52−56.

(6) Luo, J. H.; Chen, L. Y.; Nguyen, D. N.; Guo, D.; An, Q.; Cheng, M. J. J. Dual Functions of Water in Stabilizing the Metal-Pentazolate Hydrates $[M(N_5)_2(H_2O)_4]\cdot4H_2O$ (M = Mn, Fe, Co, and Zn) High-Energy Density Materials. *J. Phys. Chem. C* **2018**, *122*, 21192−21201.

(7) Bieske, E. J. Photodissociation of $(N_2)^+_n$ clusters (2≤n≤7): Branching ratios for formation of N_2^+ and N_4^+, and N_2^+ fragment vibrational excitation. *J. Chem. Phys.* **1993**, *99*, 8672−8679.

(8) Ruchti, T.; Speck, T.; Connelly, J. P.; Bieske, E. J.; Linnartz, H.; Maier, J. P. Rotationally resolved infrared absorption spectrum of N_4^+. *J. Chem. Phys.* **1996**, *105*, 2591−2594.

(9) Cacace, F.; de Petris, G.; Troiani, A. Experimental Detection of Tetranitrogen. *Science* **2002**, *295*, 480−481.

(10) Christe, K. O.; Wilson, W. W.; Sheehy, J. A.; Boatz, J. A. N_5^+: A Novel Homoleptic Polynitrogen Ion as a High Energy Density Material. *Angew. Chem., Int. Ed.* **1999**, *38*, 2004−2009.

(11) Vij, A.; Wilson, W. W.; Vij, V.; Tham, F. S.; Sheehy, J. A.; Christe, K. O. Polynitrogen Chemistry. Synthesis, Characterization, and Crystal Structure of Surprisingly Stable Fluoroantimonate Salts of N_5^+. *J. Am. Chem. Soc.* **2001**, *123*, 6308−6313.

(12) Dixon, D. A.; Feller, D.; Christe, K. O.; Wilson, W. W.; Vij, A.; Vij, V.; Jenkins, H. D. B.; Olson, R. M.; Gordon, M. S. Enthalpies of Formation of Gas Phase N_3, N_3^-, N_5^+, and N_5^- from Ab Initio Molecular Orbital Theory, Stability Predictions for $N_5^+N_3^-$ and $N_5^+N_5^-$, and Experimental Evidence for the Instability of $N_5^+N_3^-$. *J. Am. Chem. Soc.* **2004**, *126*, 834−843.

(13) Hirshberg, B.; Gerber, R. B.; Krylov, A. I. Stability and Energetics of Metastable Molecules: Tetraazatetrahedrane (N_4), Hexaazabenzene (N_6), and Octaazacubane (N_8). *J. Phys. Chem.* **1992**, *96*, 1173−1178.

(14) Hirshberg, B.; Gerber, R. B. Decomposition mechanisms and dynamics of N_6: Bond orders and partial charges along classical trajectories. *Chem. Phys. Lett.* **2012**, *531*, 46−51.

(15) Eremets, M. I.; Gavriliuk, A. G.; Trojan, I. A.; Dzivenko, D. A.; Boehler, R. Single-bonded cubic form of nitrogen. *Nat. Mater.* **2004**, *3*, 558−563.

(16) Mailhiot, C.; Yang, L. H.; McMahan, A. K. Polymeric nitrogen. *Phys. Rev. B* **1992**, *46*, 14419−14435.

(17) Mattson, W. D.; Sanchez-Portal, D.; Chiesa, S.; Martin, R. M. Prediction of New Phases of Nitrogen at High Pressure from First-Principles Simulations. *Phys. Rev. Lett.* **2004**, *93*, No. 125501.

(18) Wang, X.; Tian, F.; Wang, L.; Cui, T.; Liu, B.; Zou, G. Structural stability of polymeric nitrogen: A first-principles investigation. *J. Chem. Phys.* **2010**, *132*, No. 024502.

(19) Vij, A.; Pavlovich, J. G.; Wilson, W. W.; Vij, V.; Christe, K. O. Experimental detection of the pentaazacyclopentadienide (pentazolate) anion, cyclo-N_5^-. *Angew. Chem., Int. Ed.* **2002**, *41*, 3051−3054.

(20) Östmark, H.; Wallin, S.; Brinck, T.; Carlqvist, P.; Claridge, R.; Hedlund, E.; Yudina, L. Detection of pentazolate anion (*cyclo*-N_5^-) from laser ionization and decomposition of solid *p*-dimethylamino-phenylpentazole. *Chem. Phys. Lett.* **2003**, *379*, 539−546.

(21) Bazanov, B.; Geiger, U.; Carmieli, R.; Grinstein, D.; Welner, S.; Haas, Y. Detection of Cyclo-N_5^- in THF Solution. *Angew. Chem., Int. Ed.* **2016**, *55*, 13233−13235.

(22) Zhang, C.; Sun, C.; Hu, B.; Yu, C.; Lu, M. Synthesis and characterization of the pentazolate anion *cyclo*-N_5^- in $(N_5)_6(H_3O)_3(NH_4)_4Cl$. *Science* **2017**, *355*, 374−376.

(23) Christe, K. O. Polynitrogen chemistry enters the ring. *Science* **2017**, *355*, 351−353.

(24) Zhang, C.; Yang, C.; Hu, B.; Yu, C.; Zheng, Z.; Sun, C. A Symmetric $Co(N_5)_2(H_2O)_4 \cdot 4H_2O$ High-Nitrogen Compound Formed by Cobalt(II) Cation Trapping of a Cyclo-N_5^- Anion. *Angew. Chem., Int. Ed.* **2017**, *56*, 4512−4514.

(25) Xu, Y.; Wang, Q.; Shen, C.; Lin, Q.; Wang, P.; Lu, M. A series of energetic metal pentazolate hydrates. *Nature* **2017**, *549*, 78−81.

(26) Xu, Y.; Wang, P.; Lin, Q.; Lu, M. A Carbon-free Inorganic-metal Complex Consisting of All-nitrogen Pentazole Anion, Zn(II) Cation and H_2O. *Dalton Trans.* **2017**, *46*, 14088−14093.

(27) Xu, Y.; Lin, Q.; Wang, P.; Lu, M. Stabilization of the Pentazolate Anion in Three Anhydrous and Metal-Free Energetic Salts $(N_5^-)_2DABTT^{2+}$, N_5-GU^+, and $N_5^-Oxahy^+$. *Chem. Asian J.* **2018**, *13*, 924−928.

(28) Xu, Y.; Wang, P.; Lin, Q.; Mei, X.; Lu, M. Self-assembled energetic 3D metal-organic framework $[Na_8(N_5)_8(H_2O)_3]_n$ based on cyclo-N_5^-. *Dalton Trans.* **2018**, *47*, 1398−1401.

(29) Sun, C.; Zhang, C.; Jiang, C.; Yang, C.; Du, Y.; Zhao, Y.; Hu, B.; Zheng, Z.; Christe, K. O. Synthesis of AgN_5 and its extended 3D energetic framework. *Nat. Commun.* **2018**, *9*, 1269.

(30) Yang, C.; Zhang, C.; Zheng, Z.; Jiang, C.; Luo, J.; Du, Y.; Hu, B.; Sun, C.; Christe, K. O. Synthesis and Characterization of cyclo-Pentazolate Salts of NH_4^+, NH_3OH^+, $N_2H_5^+$, $C(NH_2)_3^+$, and $N(CH_3)_4^+$. *J. Am. Chem. Soc.* **2018**, *140*, 16488−16494.

(31) Xu, Y.; Tian, L.; Wang, P.; Lin, Q.; Lu, M. Hydrogen bonding network: stabilization of the pentazolate anion in two nonmetallic energetic salts. *Cryst. Growth Des.* **2019**, *19*, 1853−1859.

(32) Parr, R. G.; Yang, W. Density-Functional Theory of Atoms and Molecules. *Ann. Nucl. Energy* **1989**, *16*, 611−612.

(33) Zhang, L.; Jiang, S. L.; Yu, Y.; Long, Y.; Zhao, H. Y.; Peng, L. J.; Chen, J. Phase Transition in Octahydro-1,3,5,7-tetranitro-1,3,5,7-tetrazocine (HMX) under Static Compression: An Application of the First-Principles Method Specialized for CHNO Solid Explosives. *J. Phys. Chem. B* **2016**, *120*, 11510−11522.

(34) Jiang, C.; Zhang, L.; Sun, C.; Zhang, C.; Yang, C.; Chen, J.; Hu, B. Response to Comment on "Synthesis and characterization of the pentazolate anion cyclo-N_5^- in $(N_5)_6(H_3O)_3(NH_4)_4Cl$". *Science* **2018**, *359*, No. eaas8953.

(35) Zhang, L.; Yao, C.; Yu, Y.; Jiang, S.; Sun, C.; Chen, J. Stabilization of the Dual-Aromatic cyclo-N_5^- Anion by Acidic Entrapment. *J. Phys. Chem. Lett.* **2019**, *10*, 2378−2385.

(36) Methfessel, M.; Paxton, A. T. High-precision sampling for Brillouin-zone integration in metals. *Phys. Rev. B* **1989**, *40*, 3616.

(37) Perdew, J. P.; Burke, K.; Ernzerhof, M. Generalized Gradient Approximation Made Simple. *Phys. Rev. Lett.* **1996**, *77*, 3865−3868.

(38) Kohn, W.; Sham, L. J. Self-Consistent Equations Including Exchange and Correlation Effects. *J. Phys. Rev.* **1965**, *140*, A1133−A1138.

(39) Yao, C.; Yang, Y.; Yu, Y.; Sun, C. Q.; Wang, X. X.; Li, H.; Li, H.; Zhang, L. How stable and powerful can metal cyclo-pentazolate salts achieve? An answer through theoretical crystal design. *Cryst. Growth Des.* **2020**, *20*, 4794−4801.

(40) Kresse, G.; Joubert, D. From ultrasoft pseudopotentials to the projector augmented-wave method. *Phys. Rev. B* **1999**, *59*, 1758−1775.

(41) Blochl, P. E. Projector augmented-wrave method. *Phys. Rev. B* **1994**, *50*, 17953−17979.

(42) Johnson, D. A. *Metals and Chemical Change*; Royal Society of Chemistry, 2002, 1-2.

(43) Zhang, C.; Xue, X.; Cao, Y.; Zhou, J.; Zhang, A.; Li, H.; Zhou, Y.; Xu, R.; Gao, T. Toward low-sensitive and high-energetic co-crystal II: structural, electronic and energetic features of CL-20 polymorphs and the observed CL-20-based energetic−energetic co-crystals. *CrystEngComm* **2014**, *16*, 5905−5916.

(44) Wu, C. J.; Yang, L. H.; Fried, L. E.; Quenneville, J.; Martinez, T. J. Electronic structure of solid 1,3,5-triamino-2,4,6-trinitrobenzene under uniaxial compression: Possible role of pressure-induced metallization in energetic materials. *Phys. Rev. B* **2003**, *67*, No. 235101.

(45) Spackman, M. A.; Byrom, P. G. A novel definition of a molecule in a crystal. *Chem. Phys. Lett.* **1997**, *267*, 215−220.

(46) Spackman, M. A.; Jayatilaka, D. Hirshfeld surface analysis. *CrystEngComm* **2009**, *11*, 19−32.

(47) Spackman, M. A.; McKinnon, J. J. Fingerprinting intermolecular interactions in molecular crystals. *CrystEngComm* **2002**, *4*, 378−392.

(48) McKinnon, J. J.; Jayatilaka, D.; Spackman, M. A. Towards quantitative analysis of intermolecular interactions with Hirshfeld surfaces. *Chem. Commun.* **2007**, *37*, 3814−3816.

(49) McKinnon, J. J.; Spackman, M. A.; Mitchell, A. S. Novel tools for visualizing and exploring intermolecular interactions in molecular crystals. *Acta Crystallogr. B* **2004**, *60*, 627−668.

(50) Seth, S. K.; Sarkar, D.; Kar, T. Use of $\pi-\pi$ forces to steer the assembly of chromone derivatives into hydrogen bonded supramolecular layers: crystal structures and Hirshfeld surface analyses. *CrystEngComm* **2011**, *13*, 4528−4535.

(51) Lefebvre, C.; Rubez, G.; Khartabil, H.; Boisson, J. C.; Contreras-García, J.; Hénon, E. Accurately extracting the signature of intermolecular interactions present in the NCI plot of the refuced density gradient versus electron density. *Phys. Chem. Chem. Phys.* **2017**, *19*, 17928.

(52) Becke, A. D.; Edgecombe, K. E. A simple measure of electron localization in atomic and molecular systems. *J. Chem. Phys.* **1990**, *92*, 5397.

(53) Lu, T.; Chen, F. Multiwfn: A Multifunctional Wavefunction Analyzer. *J. Comput. Chem.* **2012**, *33*, 580−592.

(54) Johnson, E. R.; Keinan, S.; Mori-Sánchez, P.; Contreras-García, J.; Cohen, A. J.; Yang, W. Revealing noncovalent interactions. *J. Am. Chem. Soc.* **2010**, *132*, 6498−6506.

(55) Lu, T.; Chen, F. Bond Order Analysis Based on the Laplacian of Electron Density in Fuzzy Overlap Space. *J. Phys. Chem. A* **2013**, *117*, 3100−3108.